




Open Archive Toulouse Archive Ouverte (OATAO)

OATAO is an open access repository that collects the work of some Toulouse researchers and makes it freely available over the web where possible.

This is an author's version published in: <https://oatao.univ-toulouse.fr/23419>

Official URL : <https://doi.org/10.1016/j.proci.2018.05.108>

To cite this version :

Genot, Aurelien and Gallier, Stany and Schuller, Thierry  *Thermo-acoustic instabilities driven by fuel droplet lifetime oscillations*. (2018) *Proceedings of the Combustion Institute*, 37 (4). 5359-5366. ISSN 1540-7489

Any correspondence concerning this service should be sent to the repository administrator:

tech-oatao@listes-diff.inp-toulouse.fr

Thermo-acoustic instabilities driven by fuel droplet lifetime oscillations

Aurelien Genot^{a, b, c, *}, Stany Gallier^b, Thierry Schuller^{c, d}

^a *CNES DLA, Centre National d'Etudes Spatiales, Direction des Lanceurs, 52 rue Jacques Hillairet, Paris cedex 75612, France*

^b *ArianeGroup, Le Bouchet Research Center, 9 rue Lavoisier, Vert-le-Petit 91710, France*

^c *Laboratoire EM2C, CNRS, CentraleSupélec, Université Paris Saclay, 3 rue Joliot Curie, Gif-sur-Yvette 91190, France*

^d *Institut de Mécanique des Fluides de Toulouse, IMFT, Université de Toulouse, CNRS, Toulouse, France*

Abstract

A new mechanism of thermo-acoustic destabilization of combustors powered by burning droplets is investigated. Acoustic induced heat release disturbances are found to be driven by oscillations of droplet lifetime during the final stage of the droplet combustion before their extinction. The mechanism is the following. Synchronized acoustic disturbances alter the droplet evaporation rate and modify their diameter. Perturbations of the droplet diameter along the droplet trajectories lead to fluctuations of their lifetime. These fluctuations trigger in turn an oscillating motion of the burning droplet cloud boundary that is synchronized by the acoustic excitation. This leads to large heat release fluctuations before droplet extinction and constitutes a thermo-acoustic source. This mechanism is found to be particularly important in solid rocket motors in which aluminum droplets released from the propellant burn individually and are quenched as the droplet diameter falls below a critical residue diameter associated to an inert particle. Analytical models are derived in an idealized configuration where acoustic forcing takes place in the transverse direction to the droplet trajectories. Expressions are derived in the frequency space for the droplet diameter oscillations, the motion of the droplet cloud boundary and the resulting heat release disturbances, that take the form of a distributed Flame Describing Function. This model is used to reveal effects of the acoustic pressure level and of the residue diameter on the resulting motion of the combustion volume boundary and corresponding heat release disturbances. It is further extended to consider the peculiar flow in a solid rocket motor and the heat release disturbance model is compared to results from numerical flow simulations of the motor. While highlighted in the context of solid propulsion, the observations made are believed to be more general and the same mechanisms may persist in acoustically perturbed spray flames from hydrocarbon fuel droplets.

Keywords: Droplet combustion; Flame Describing Function; Thermo-acoustic instability; Solid rocket motor

1. Introduction

Aero and rocket engines are prone to combustion instabilities [1–3]. In systems powered by fuel sprays, acoustic oscillations may trigger mixture fraction disturbances (i) by modifying the droplet size distribution at the injector inlet [4,5], (ii) by segregation of large from small droplets during their transport in the pulsed flow [6] and (iii) by reducing the droplet evaporation time due to the additional drag from the pulsed flow [7–9]. Each of these mechanisms alter the flame dynamics.

In numerical simulations of liquid propellant rocket engines, transverse acoustic oscillations were shown to lead to shorter flames due to acceleration of mixing and evaporation of the propellant injected as liquid droplets [10], a phenomenon which is also observed in experiments and simulations conducted at transcritical conditions [11,12]. Longitudinal high-amplitude acoustic oscillations were also found to reduce the length of liquid fuel sprays [13]. Carvalho et al. [7] observed a reduction in the mean droplet lifetime due to acoustic forcing in their numerical model of a Rijke tube burning liquid droplets. Blaszczyk [14] showed experimentally a dependence of the droplet consumption rate and of the mean droplet lifetime on the acoustic amplitude and frequency. These different studies reveal that acoustic oscillations interacting with fuel droplets often lead to changes of the spray and flame structures.

A new contribution to heat release rate fluctuations associated to oscillations of the droplet lifetime is investigated in this study. These disturbances are shown to constitute an additional thermo-acoustic source of destabilization of the combustor. The mechanism is reminiscent of the displacement of a flame interface in an acoustic field as observed in some high frequency instabilities coupled to transverse modes [10,15].

This article focuses on aluminum burning droplets in an acoustic field transverse to the droplet trajectory, because the phenomenon has been recently highlighted in solid rocket motors (SRMs) [16,17], but the analytical results are valid for any system with quasi one dimensional droplet trajectories burning individually.

Flame quenching induced by acoustic excitation [18] is not considered in this study in which acoustic disturbances remain small and in the linear regime. Also, the acoustic radiation force [19] can be neglected in comparison with the drag force exerted by the flow. With these hypotheses, droplet lifetime and its fluctuations are only driven by changes of the mass consumption rate along the droplet trajectory. A reduction of the mean droplet lifetime may also be observed in numerical simulations at high acoustic levels, but the following study is limited to the low-amplitude acoustic response in which case the mean droplet lifetime remains invariant.

The article is organized as follows. Section 2 highlights the mechanism identified in a generic SRM featuring a self-sustained thermo-acoustic instability. Section 3 develops the analytical model in an idealized configuration with a uniform flow. The analytical approach is extended to include SRM specificities and is compared to simulation results in Section 4.

2. Illustration in a SRM

It was recently shown that the combustion dynamics of aluminum droplets may lead to self-sustained thermo-acoustic oscillations in SRM [16,17]. In these simulations, dilute aluminum droplet combustion is modeled by the D^2 law (group combustion is neglected [20–22]):

$$\frac{dD^2}{dt} = -\frac{4\mu \ln(1+B)\text{Sh}}{\rho_p \text{Pr}} \quad (1)$$

with D the fuel droplet diameter, ρ_p the droplet density, μ the gas viscosity, Pr the Prandtl number, B the Spalding number taken from [16] and Sh the Sherwood number. To reproduce experimental observations [21], the combustion reaction is stopped when the particle diameter reaches the aluminum oxide residue diameter D_r :

$$\dot{q} = \dot{q}_{D^2} \mathcal{H}(D - D_r) \quad (2)$$

where \mathcal{H} is the Heaviside function and \dot{q}_{D^2} denotes the rate of heat released from N_p droplets per unit volume which are burning individually and are moving with a velocity \mathbf{u}_p in a gas flow at velocity \mathbf{u} . The burning rate is enhanced by flow convection around the fuel droplets:

$$\dot{q}_{D^2} = N_p \Delta h_r \pi D \frac{\mu}{\text{Pr}} \ln(1+B)\text{Sh} \quad (3)$$

where Δh_r is the reaction enthalpy and the Sherwood number Sh is deduced from the Ranz–Marshall correlation [23]:

$$\text{Sh} = 2 + 0.6 \text{Re}_p^{1/2} \text{Pr}^{1/3} \quad \text{Re}_p = \frac{\rho_g |\delta \mathbf{u}_p| D}{\mu} \quad (4)$$

with ρ_g the gas density and $|\delta \mathbf{u}_p| = |\mathbf{u}_p - \mathbf{u}|$ the norm of the particle relative velocity. In the case of a uniform flow, the lifetime of the burning droplet is given by:

$$t_c = \frac{\rho_p \text{Pr} (D_i^2 - D_r^2)}{4\mu \ln(1+B)\text{Sh}} \quad (5)$$

where D_i and D_r are the initial and residual diameters of the fuel droplet. Transient droplet heating is neglected, the droplet temperature being considered constant and equal to the saturation temperature.

An example of simulation in a thermo-acoustically unstable state is now briefly described to illustrate the system dynamics. More details about the numerical flow model are given in

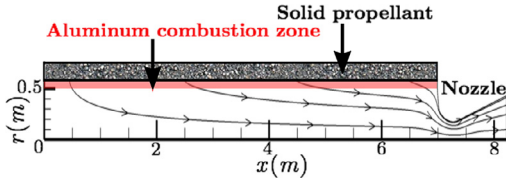


Fig. 1. Cylindrical solid rocket motor (SRM) geometry and computed gas streamlines in the numerical domain. (For interpretation of the references to color in this figure legend, the reader is referred to the web version of this article.)

Section 4.1. Figure 1 shows the gas streamlines of the mean flow and delineates the aluminum combustion zone in the numerical flow domain. The SRM chamber has a length $L = 7$ m and a constant radius $R = 0.593$ m. Propellant burning is modeled with an imposed burning rate normal to the propellant boundary. Aluminum droplets are injected radially, from the solid propellant wall at $r = R$ at the gas phase velocity $\mathbf{u}_p = \mathbf{u}$ and burn in the boundary layer along the solid propellant. A single class of droplets is injected with an initial diameter D_i taken from the baseline configuration of [16] and the residual diameter is fixed to $D_r = D_i/2$.

Figure 2 illustrates the dynamics of the SRM during one oscillation cycle. The combustion os-

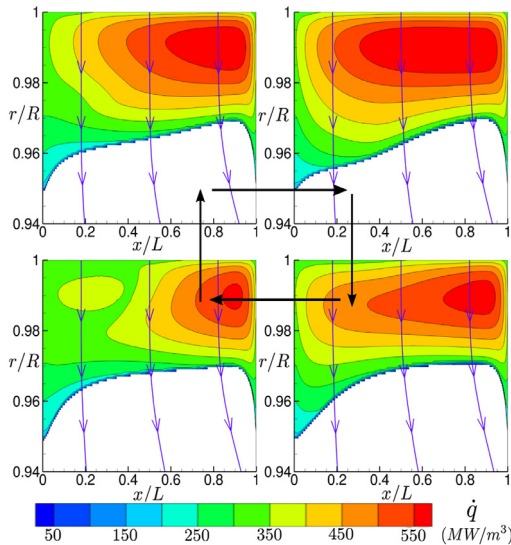


Fig. 2. Heat release rate distribution \dot{q} in the cylindrical chamber of a SRM at four regularly distributed instants of a limit cycle of a thermo-acoustic instability driven by aluminum droplet combustion. A few droplet streamlines are superimposed in blue. The radial coordinate is stretched here so as to make the thin aluminum droplet combustion zone more visible. (For interpretation of the references to color in this figure legend, the reader is referred to the web version of this article.)

cillation is here coupled to the first longitudinal acoustic mode of the motor. The droplet streamlines in Fig. 2 have a quasi 1D-trajectory normal to the aluminum combustion zone. Close to the nozzle for $0.5 \leq x/L \leq 1$, the volumetric heat release rate \dot{q} takes higher values and the volume occupied by the burning droplets is thinner than in the first section of the motor, due to higher flow velocities. Longitudinal fluctuations of the volumetric heat release rate \dot{q} can also be clearly identified in the combustion volume. This contribution is associated to disturbances of the combustion rate of aluminum droplets due to acoustic velocity fluctuations as described in [9,16]. Also, a flapping motion of the boundary between the combustion zone and the inert zone (white region in Fig. 2) is remarkable. This motion essentially takes place in the radial direction, while the acoustic mode is controlled by longitudinal acoustic oscillations.

This simulation is further analyzed by examining the local Rayleigh index \mathcal{S} [24] corresponding to the thermo-acoustic source coupling acoustic pressure p_1 and heat release rate \dot{q}_1 fluctuations. This index is plotted in Fig. 3 over the entire flow. As the instability is locked on the first acoustic mode, aluminum combustion produces pressure oscillations ($\mathcal{S} > 0$) close to the head end, whereas pressure oscillations are damped close to the nozzle ($\mathcal{S} < 0$). The low frequency pressure fluctuations are invariant in the radial direction [16], and the radial variations observed for the Rayleigh index in Fig. 3 are due to heat release rate fluctuations.

The high values of the Rayleigh index at the aluminum combustion zone contribute up to 30% of the global Rayleigh index $\int_V \mathcal{S} dV$ integrated over the whole flow volume V [22]. They are due to the flapping motion of the combustion volume boundary observed in Fig. 2, which

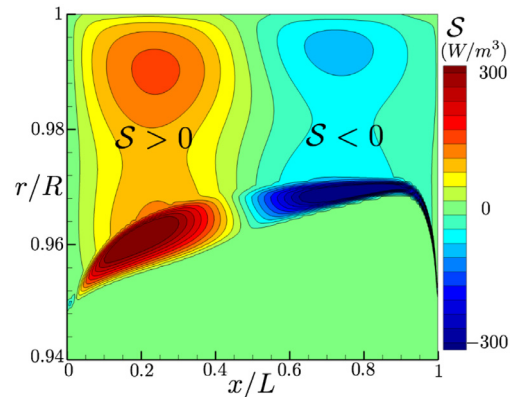


Fig. 3. Distribution of the local Rayleigh index $\mathcal{S} = \frac{\gamma-1}{\gamma p_0 T} \int_T p_1 \dot{q}_1 dt$ through the SRM. T is the acoustic period ($T = 1/f$), γ the specific heat ratio, p_0 the mean pressure, p_1 the pressure fluctuations and \dot{q}_1 the heat release rate fluctuations.

is itself associated to the dynamics of aluminum droplets as they reach their residual diameters. It is demonstrated in this study that the heat release fluctuations originating from the combustion volume boundary result from oscillations of aluminum droplet lifetime. An analytical model is developed to determine the resulting heat release disturbances. The heat release rate fluctuations produced inside the combustion volume are deliberately discarded in the following analytical developments to better highlight the contribution from the boundary. This leads to neglecting the fluctuations of \dot{q}_{D^2} in Eq. (2).

3. Analytical model

The model aims at reproducing the heat release fluctuations associated with droplet lifetime oscillations and at identifying the main parameters controlling this dynamics. It is developed for harmonic, linear and low frequency traveling or standing sound waves. Droplet lifetime oscillations are driven by their dynamics as they approach the residue droplet diameter $D = D_r$. A linear model for perturbations of the droplet lifetime is derived from Eq. (1) and reads in the Fourier space:

$$\hat{i}_c = \frac{2t_{c,0}D_0}{D_i^2 - D_r^2} \hat{D} \quad (6)$$

where $\hat{\cdot}$ denotes the Fourier component of the perturbation at frequency f . In the following, the subscript 0 designates the mean value and the subscript 1 stands for the perturbed state: $X(t) = X_0 + X_1(t)$, where $X_1 = \mathcal{R}_e(\hat{X} \exp(i\omega t))$, \mathcal{R}_e denotes the real part and $\omega = 2\pi f$ the angular frequency.

3.1. Idealized configuration

The problem is not directly tackled on the SRM but first examined on a simpler and idealized configuration which reproduces the main features of the dynamics observed in SRMs. One considers the configuration sketched in Fig. 4. Fuel droplets are released vertically at $y = 0$ in an oxidizer gaseous stream characterized by a uniform mean velocity u_0 plus a harmonic fluctuation u_1 in the axial direction. Droplet trajectories are assumed to be quasi-1D, with a small axial particle velocity compared to their vertical component $u_p \ll v_p$. The mean diameter D_0 is taken here, as a first approximation, as the mean value between the initial and the residue value. The combustion zone boundary is delimited by y_c in Fig. 4:

$$y_c = v_p t_c \quad (7)$$

where v_p is the vertical droplet velocity, which is here taken constant. In this model, the boundary y_c moves if the droplet lifetime fluctuates and this motion leads in turn to heat release rate fluctuations.

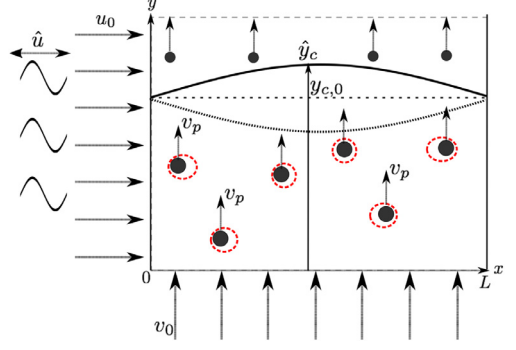


Fig. 4. Isolated burning droplets crossing an uniform flow in the transverse direction, which is acoustically perturbed.

Equation (2) can be rewritten as:

$$\dot{q} = \dot{q}_{D^2,0} \mathcal{H}(D(t) - D_r) = \dot{q}_{D^2,0} \mathcal{H}(y_c(t) - y) \quad (8)$$

where y_c designates the position verifying $D = D_r$. At the boundary y_c , one has:

$$\frac{\partial \dot{q}}{\partial t} = \frac{\partial y_c}{\partial t} \dot{q}_{D^2,0} \delta(y_c(t) - y) \quad (9)$$

where δ denotes the Dirac distribution. This equation is reminiscent of expressions of heat release disturbances associated to high frequency transverse flow disturbances [10,15]. The next step is to link the disturbances of the boundary y_c to disturbances of the droplet fuel diameter D , which depends itself on the gas velocity u .

At low forcing frequencies, the droplet response to acoustic perturbations remains quasi-steady [4,9,25] and effects of acoustic pressure, gas temperature, gas density and number of droplets disturbances can be neglected [8,16]. The droplet lifetime, as the heat release rate, is only altered by fluctuations of the droplet diameter D , droplet velocity u_p and gas velocity u .

The following expressions are derived for small disturbances linking the particle velocity u_p and the droplet diameter D to the gas velocity u . The derivation is based on the system of conservative Eulerian equations given by Gallier and Godfroy [16].

For disturbances of the droplet axial velocity $u_{p,1}$, one is left with:

$$\frac{\partial u_{p,1}}{\partial t} = -\frac{\delta u_{p,1}}{\tau_{v,0}} + \frac{\delta u_{p,0} \tau_{v,1}}{\tau_{v,0}^2} \quad (10)$$

where $\delta u_p = u_p - u$ is the difference between the axial particle and gas velocities and τ_v is the droplet relaxation time given by [16,26]:

$$\tau_v = \frac{1 + B}{1 + 0.15 \text{Re}_p^{0.687}} \frac{\rho_p D^2}{18\mu} \quad (11)$$

Gradients acting on velocity disturbances are neglected in Eq. (10) by setting $\nabla u_{p,1} = 0$.

Equation (1) is now used to determine a transport equation for disturbances D_1 of the droplet diameter in an Eulerian framework:

$$\frac{\partial D_1}{\partial t} + v_p \frac{\partial D_1}{\partial y} = -\frac{(D_i^2 - D_r^2)}{2D_0 t_{c,0}} \left(\frac{\text{Sh}_1}{\text{Sh}_0} - \frac{D_1}{D_0} \right) \quad (12)$$

For small oscillations at the frequency f , Eq. (10) yields in the Fourier space:

$$\hat{u}_p \left(i\omega\tau_{v,0} + 1 + \frac{C_{Re}\delta u_{p,0}^2}{|\delta \mathbf{u}_{p,0}|^2} \right) = \hat{u} \left(1 + \frac{C_{Re}\delta u_{p,0}^2}{|\delta \mathbf{u}_{p,0}|^2} \right) + \frac{\hat{D}}{D_0} \delta u_{p,0} (2 - C_{Re}) \quad (13)$$

where C_{Re} is a mean quantity due to fluctuations of the drag characteristic time:

$$C_{Re} = \frac{0.687 \times 0.15 \text{Re}_{p,0}^{0.687}}{1 + 0.15 \text{Re}_{p,0}^{0.687}} \quad (14)$$

Fluctuations of the droplet diameter given by Eq. (12) obey in the Fourier space to:

$$\frac{\partial \hat{D}}{\partial y} + \hat{D} \left(\frac{i\omega}{v_p} - \frac{(\text{Sh}_0 + 2)(D_i^2 - D_r^2)}{4v_p t_{c,0} \text{Sh}_0 D_0^2} \right) = -\frac{(\text{Sh}_0 - 2)(D_i^2 - D_r^2)}{4v_p t_{c,0} \text{Sh}_0 D_0 |\delta \mathbf{u}_{p,0}|^2 / \delta u_{p,0}} (\hat{u}_p - \hat{u}) \quad (15)$$

In the absence of diameter fluctuations at the injection boundary $y = 0$, substitution of Eq. (13) in Eq. (15), assuming a mean uniform flow, yields the transfer function linking the droplet diameter to the axial gas stream velocity fluctuation:

$$\frac{\hat{D}}{D_0} = \frac{K_B}{K_A} (1 - e^{K_A y / D_0}) \frac{\hat{u}}{\delta u_{p,0}} \quad (16)$$

where K_A and K_B are constant numbers that only depend on the mean flow properties:

$$K_A = \frac{i\omega D_0}{v_p} - \frac{(D_i^2 - D_r^2)/D_0}{4v_p t_{c,0} \text{Sh}_0} \times \left(\text{Sh}_0 + 2 - \frac{(\text{Sh}_0 - 2)(2 - C_{Re}) \frac{\delta u_{p,0}^2}{|\delta \mathbf{u}_{p,0}|^2}}{(i\omega\tau_{v,0} + 1 + \frac{C_{Re}\delta u_{p,0}^2}{|\delta \mathbf{u}_{p,0}|^2})} \right) \quad (17)$$

$$K_B = -\frac{(D_i^2 - D_r^2)(\text{Sh}_0 - 2)i\omega\tau_{v,0}}{4v_p t_{c,0} D_0 \text{Sh}_0 |\delta \mathbf{u}_{p,0}|^2 / \delta u_{p,0}^2} \quad (18)$$

The dynamics of the combustion zone boundary y_c where the droplet diameter has reached the residue diameter $D = D_r$ is deduced from Eqs. (6) and (7):

$$\hat{y}_c = v_p \hat{t}_c = \frac{2t_{c,0} v_p D_0}{D_i^2 - D_r^2} \hat{D} \quad y_{c,0} = v_p t_{c,0} \quad (19)$$

Table 1
Model input parameters.

μ	$9.1 \cdot 10^{-5}$ kg/m/s	Pr	0.4
D_0	$\frac{D_i + D_r}{2}$	v_0	0 m/s
$\delta u_{p,0}$	1 m/s	v_p	2 m/s
B	1	p_0	10^7 Pa
ρ_g	10 kg/m ³	γ	1
$a_0 = (\frac{\gamma p_0}{\rho_g})^{1/2}$	1000 m/s	L	10 m
ρ_p	2000 kg/m ³	f	50 Hz

where droplet diameter disturbances \hat{D} are given by Eq. (16). Taking the Fourier transform of Eq. (9), one finally finds for the resulting heat release rate disturbances:

$$\frac{\hat{q}}{\hat{q}_{D^2,0}} = F_y \hat{y}_c, \quad F_y = \frac{2 \left(1 - \left(\frac{y - y_{c,0}}{|\hat{y}_c|} \right)^2 \right)^{1/2}}{\pi |\hat{y}_c|} \quad (20)$$

This expression yielding the volumetric heat release rate response to the acoustic forcing is non-linear because the transfer function F_y depends on the amplitude of the motion of y_c . This is due to the Dirac distribution appearing in Eq. (9). Equation (20) thus corresponds to a distributed Flame Describing Function [27].

3.2. Parametric analysis

The model derived in the previous section is now used to examine effects of the residual particle diameter D_r and acoustic pressure amplitude $\hat{\eta}$ on the motion of the combustion boundary \hat{y}_c and the resulting heat release rate disturbances \hat{q} . The input parameters for the calculations are synthesized in Table 1 and are selected to mimic conditions prevailing in a SRM, except v_0 sets to zero to maximize convection effects.

One also chooses here to mimic the modal structure of the acoustic field observed in an acoustically closed-closed chamber, as a SRM chamber, undergoing a self-sustained thermo-acoustic oscillation at $f = 50$ Hz coupled to the first longitudinal 1L mode, with droplets injected in the transverse direction. The Fourier component \hat{u} of the axial acoustic velocity vanishes at $x = 0$ and $x = L$ and is expressed as [1]:

$$\hat{u} = \frac{-i\hat{\eta}}{a_0 \rho_g} \sin(kx) \quad (21)$$

where $\hat{\eta}$ is the acoustic pressure amplitude and $k = 2\pi f/a_0$ the wave number and a_0 the speed of sound.

Model results are shown in Fig. 5 for three acoustic pressure levels $\hat{\eta} = 10^3, 5 \cdot 10^3$ and 10^4 Pa and a residue diameter $D_r = D_i/2$ equal to half the initial aluminum droplet diameter. The evolution of the modulus of the relative heat release rate fluctuation $|\hat{q}|/\hat{q}_{D^2,0}$ calculated with Eq. (20) is plotted

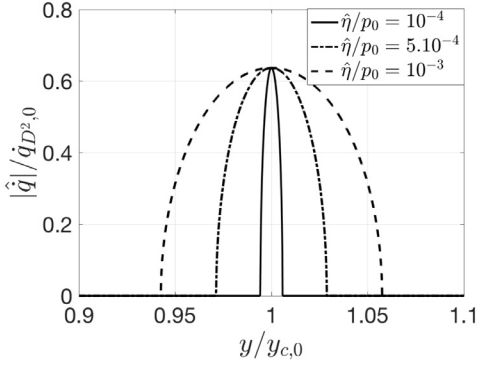


Fig. 5. Heat release rate fluctuations around the combustion volume boundary $y_{c,0}$ at $x/L = 1/4$ for different pressure levels $\hat{\eta} = 10^3$, 5.10^3 and 10^4 Pa. The residue diameter is fixed to $D_r = D_i/2$.

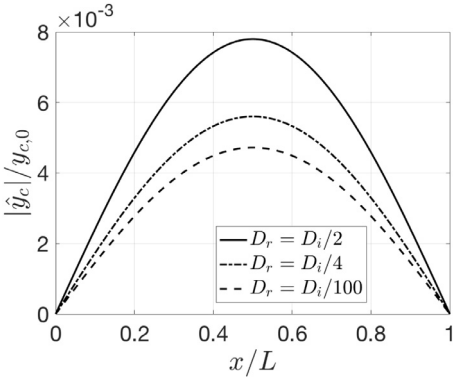


Fig. 6. Modulus of the motion of the combustion volume boundary for different residue diameters D_r . The acoustic pressure level is fixed to $\hat{\eta} = 10^3$ Pa.

along the y -axis for a cut at $x/L = 1/4$. This figure shows that heat release disturbances associated to droplet lifetime oscillations only take place close to the mean position of the combustion volume boundary $y_{c,0}$. The motion amplitude increases as the acoustic pressure level rises in the chamber, whereas the heat release rate fluctuation peak value remains independent of the pressure level.

The impact of the residue diameter is investigated in Fig. 6 by considering three different residue to initial diameter ratios, and an acoustic pressure oscillation level fixed to $\hat{\eta} = 10^3$ Pa. The amplitude of the displacement \hat{y}_c of the combustion boundary increases as the size of the residue diameter D_r increases. It nonetheless does not vanish even for small residues when $D_r = D_i/100$ (dashed lines) meaning that even for complete evaporation of the droplets, as for example in the case of liquid hydrocarbon fuel droplets burning in air, a motion of the combustion boundary persists due to droplet lifetime oscillations. For small residue diameters, the

resulting heat release fluctuations remain however small at the boundary. For high residue diameters, as for example for aluminum droplet combustion, droplet lifetime oscillations may lead to large heat release rate fluctuations.

4. Application to a cylindrical SRM

The previous model has been derived for a uniform gaseous flow in a 2D context. It can easily be extended to non-uniform flows in 2D axisymmetric geometries, considering slight changes of the analytical formalism, which are not reproduced here for concision. Analytical predictions are compared to numerical flow simulations in a SRM configuration.

4.1. Numerical model

The simulation is carried out in a 2D axisymmetric framework with the numerical model from [16]. A cylindrical motor, with a radial injection of mass modeling the solid propellant combustion (gas and aluminum droplets) and with a nozzle, is simulated with CPS, an in-house ArianeGroup flow solver [28]. The configuration is shown in Fig. 1. The chamber has a radius $R = 0.593$ m, a length $L = 7$ m and a symmetry axis at $r = 0$. The nozzle has a throat of radius $R_t = 0.175$ m, which is located at $x_t = 7.3$ m away from the motor head-end $x = 0$. The computational grid is composed of 360,000 quads with about 600 points in the axial direction and 600 points in the radial direction. The grid is clustered near the propellant burning surface to resolve the aluminum distributed combustion indicated in red in Fig. 1, with about 20 grid points in the flapping zone (Fig. 3). The smallest grid spacing at the propellant surface is about 0.1 mm. Gas and aluminum particle properties are taken from [16,29]. It is worth mentioning that turbulence is not taken into account in this simulation to focus the analysis on the coupling between acoustics and aluminum droplet unsteady combustion.

No-slip conditions are used for the gaseous and particle phases at the wall boundaries. Solid propellant burning ($r = R$) is modeled through the lateral boundary of the numerical domain between $x = 0$ and L by injection of gas at a constant mass flow rate with a velocity vector normal to the surface and pointing inward. Only a single class of droplets is considered with an initial diameter D_i taken from the baseline configuration of [16] and the aluminum oxide residue diameter is fixed to $D_r = D_i/2.4$. Aluminum particles are injected at the dynamic equilibrium with the gas $\mathbf{u}_{p,i} \cdot \mathbf{e}_r = \mathbf{u}_i \cdot \mathbf{e}_r$. This configuration is found to be thermoacoustically stable. A pulsation of 5000 Pa is imposed at the head-end boundary. This forcing level is small enough to assume linear fluctuations of the flow variables.

4.2. Model validation

Aluminum droplets are injected uniformly and radially at the solid propellant boundary at $r = R$ and the aluminum combustion takes place very close to the solid propellant surface as illustrated in red in Fig. 1. The small thickness of the combustion volume allows to assume a quasi-1D trajectory in the radial direction of the aluminum droplets which are released within the flow.

In a SRM, the mean flow field is not uniform and the longitudinal velocity fluctuations also depend on the radial position within the motor due to the particular structure of the acoustic boundary layer in these systems with mass injection from the lateral walls [1,30,31]. Due to these complexities, the expressions derived in the previous section are not valid, but analytical solutions to Eqs. (13) and (15) can still be obtained assuming a one-dimensional droplet trajectory and neglecting the influence of the droplet diameter fluctuations on the droplet velocity fluctuations.

Equation (19) remains unchanged in this new configuration:

$$\hat{r}_c = \frac{2t_{c,0}v_p D_0}{D_i^2 - D_r^2} \hat{D} \quad (22)$$

where \hat{r}_c corresponds to the Fourier component of the radial displacement of the combustion boundary in Fig. 1 at the frequency f . The mean position $r_{c,0}$ of this boundary in a non-uniform flow is:

$$r_{c,0} = R + \frac{2}{D_i^2 - D_r^2} \int_{D_i}^{D_r} t_{c,0}v_p D_0 dD \quad (23)$$

The corresponding heat release rate fluctuation is identically given by (no difference between 2D and 2D axisymmetric configurations):

$$\frac{\hat{q}}{\hat{q}_{D^2,0}} = - \frac{2 \left(1 - \left(\frac{r-r_{c,0}}{|r_c|} \right)^2 \right)^{1/2}}{\pi |\hat{r}_c|} \hat{r}_c \quad (24)$$

Figures 7 and 8 compare the modulus and phase lag of the heat release rate fluctuations taken from the numerical flow simulation and from Eq. (24) at two positions $x/L = 1/4$ and $x/L = 3/4$ in the SRM. To be fully consistent, the mean quantities appearing in the different analytical expressions are here taken from the simulation. The phase lag in Fig. 8 is expressed with respect to the acoustic pressure. The numerical data from the flow solver are well reproduced by the analytical model at the end of the combustion zone (where the boundary is oscillating) at both positions $x/L = 1/4$ and $x/L = 3/4$ in the motor chamber. One recalls that the heat release rate fluctuations taking place inside the combustion volume are voluntarily not considered in the analytical model developed in this study. The same match between analytical and numerical data is found at the other positions in the SRM confirming that the model well reproduce the flow

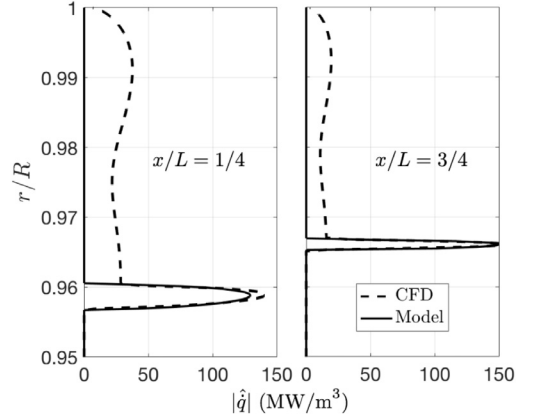


Fig. 7. Comparison between numerical flow simulations and analytical results for the modulus $|\hat{q}|$ of the heat release rate fluctuations at $x/L = 1/4$ and $x/L = 3/4$. Only the contribution originating from the boundary is modeled here.

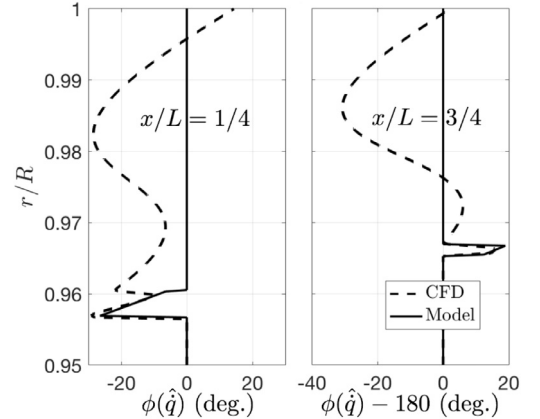


Fig. 8. Comparison between numerical flow simulations and analytical results for the phase lag ϕ of the heat release rate fluctuations \hat{q} with respect to the acoustic pressure at $x/L = 1/4$ and $x/L = 3/4$. Only the boundary contribution is modeled here.

simulations and that droplet lifetime oscillations constitute a source of unsteady heat release at the boundary of the combustion volume. This contribution to the overall heat release oscillation is found to be particularly high in simulations carried out with aluminum droplets in which combustion is abruptly quenched [22].

5. Conclusion

Distributed combustion of fuel droplets has been modeled by the D^2 law and is abruptly stopped when the droplet diameter falls below a residual diameter D_r . This is used to model the existence of

combustion residues, as the ones produced by aluminum burning droplets. It has been shown that the response of this model to acoustic disturbances leads to large heat release rate oscillations. These oscillations have been found to be related to oscillations of the lifetime of the burning droplets leading to a motion of the combustion volume boundary. A series of analytical expressions have been derived for the fluctuations of the droplet lifetime as a function of the droplet diameter fluctuations, which have been themselves related to acoustic velocity fluctuations of the gaseous phase. For droplets released in the transverse direction to the acoustic forcing, it has been demonstrated that oscillations of the droplet lifetime lead to a motion of the iso-line $D = D_r$. If the heat release rate at this iso-line remains finite, high levels of fluctuations can be observed. The heat release rate response associated to the motion of this boundary has been modeled by a Heaviside function and a distributed Flame Describing Function in the Fourier space. Finally, this model has been successfully compared with numerical flow simulations in a solid rocket motor configuration in which the combustion of acoustically perturbed droplets may be quenched.

Acknowledgments

This work is cofunded by the French space agency Centre National d'Etudes Spatiales (CNES) and ArianeGroup.

References

- [1] F. Culick, *Unsteady Motions in Combustion Chambers for Propulsion Systems*, 2006, AGARDograph, NATO/RTO-AG-AVT-039.
- [2] Lieuwen T.C., V. Yang (Eds.), *Combustion Instabilities in Gas Turbine Engines: Operational Experience, Fundamental Mechanisms and Modeling*, 2005. Progress in Astronautics and Aeronautics, AIAA, Vol. 210.
- [3] S. Candel, D. Durox, T. Schuller, N. Darabiha, L. Hakim, T. Schmitt, *Eur. J. Mech. B/Fluids* 40 (2013) 87–106.
- [4] M. Zhu, A. Dowling, K. Bray, *J. Eng. Gas Turb. Power* 124 (2002) 20–30.
- [5] J. Eckstein, E. Freitag, C. Hirsch, T. Sattelmayer, R.V.d. Bank, T. Schilling, *J. Eng. Gas Turb. Power* 127 (2005) 301–306.
- [6] F. Giuliani, P. Gajan, O. Diers, M. Ledoux, *Proc. Combust. Inst.* 29 (2002) 91–98.
- [7] J. Carvalho, M. McQuay, P. Gotac, *Combust. Flame* 108 (1997) 87–103.
- [8] K.P. Brooks, M.W. Beckstead, *J. Prop. Power* 11 (1995) 769–780.
- [9] S. Gallier, F. Sibe, O. Orlandi, *Proc. Combust. Inst.* 33 (2011) 1949–1956.
- [10] T. Sattelmayer, M. Schmid, M. Schulze, *J. Spacecr. Rockets* 52 (2015) 1417–1429.
- [11] Y. Méry, L. Hakim, P. Scoufflaire, L. Vingert, S. Ducruix, S. Candel, *C.R. Mécanique* 341 (2013) 100–109.
- [12] L. Hakim, T. Schmitt, S. Ducruix, S. Candel, *Combust. Flame* 162 (2015) 3482–3502.
- [13] R. Sujith, *Exp. Fluids* 38 (2005) 576–587.
- [14] J. Blaszczyk, *Fuel* 70 (1991) 1023–1025.
- [15] Y. Méry, *Proc. Combust. Inst.* 36 (2017) 3889–3898.
- [16] S. Gallier, F. Godfroy, *J. Prop. Power* 25 (2009) 509–521.
- [17] O. Orlandi, M. Plaud, F. Godfroy, S. Larrieu, N. Cesco, *Eucass Paper EUCASS2017-532* (2017).
- [18] D. McKinney, D. Dunn-Rankin, *Combust. Sci. Technol.* 161 (2000) 27–48.
- [19] M. Tanabe, T. Morita, K. Aoki, K. Satoh, T. Fujimori, J. Sato, *Proc. Combust. Inst.* 28 (2000) 1007–1013.
- [20] V.K. Bind, S. Roy, C. Rajagopal, *Chem. Eng. J.* 207 (2012) 625–634.
- [21] M.W. Beckstead, *A Summary of Aluminum Combustion*, 2004. NATO Report RTO-EN-023. Brigham Young University Provo, Utah, USA.
- [22] A. Genot, S. Gallier, T. Schuller, *Eucass Paper EUCASS2017-064* (2017).
- [23] W.E. Ranz, W.R. Marshall, *Chem. Eng. Prog.* 48 (1952) 141–146.
- [24] D. Durox, T. Schuller, N. Noiray, A.L. Birbaud, S. Candel, *Combust. Flame* 156 (2009) 106–119.
- [25] M. Zhu, A. Dowling, K. Bray, *J. Eng. Gas Turb. Power* 123 (2001) 779–786.
- [26] J.R. Grace, R. Clift, M.E. Weber, *Bubbles, Drops, and Particles*, Academic Press, New York, 1978.
- [27] N. Noiray, D. Durox, T. Schuller, S. Candel, *J. Fluid Mech.* 615 (2008) 139–167.
- [28] P. Durand, B. Vieille, H. Lambare, H. Vuillermoz, P. Boure, G. Steinfield, F. Godfroy, J.F. Guéry, *CPS - A three dimensional CFD code devoted to space propulsive flows*, 36th AIAA/ASME/SAE/ASEE Joint Propulsion Conference and Exhibit, Las Vegas, NV, USA, 2000.
- [29] J. Dupays, F. Vuillot, *Propagation of an acoustic wave in a two-phase reactive medium*, 34th AIAA/ASME/SAE/ASEE joint Propulsion Conference and Exhibit, Academic Press, Cleveland, OH, 1998.
- [30] W. Cai, V. Yang, G.A. Flandro, *Solid Propellant Chemistry, Combustion, and Motor Interior Ballistics*, in Progress in Astronautics and Aeronautics, AIAA, 185, 2000, pp. 837–858.
- [31] G.A. Flandro, *J. Prop. Power* 11 (1995) 607–625.